nature nanotechnology

LETTERS

PUBLISHED ONLINE: 19 FEBRUARY 2012 | DOI: 10.1038/NNANO.2012.21

A single-atom transistor

Martin Fuechsle[1], Jill A. Miwa[1], Suddhasatta Mahapatra[1], Hoon Ryu[2], Sunhee Lee[3], Oliver Warschkow[4], Lloyd C. L. Hollenberg[5], Gerhard Klimeck[3] and Michelle Y. Simmons[1]*

The ability to control matter at the atomic scale and build devices with atomic precision is central to nanotechnology. The scanning tunnelling microscope[1] can manipulate individual atoms[2] and molecules on surfaces, but the manipulation of silicon to make atomic-scale logic circuits has been hampered by the covalent nature of its bonds. Resist-based strategies have allowed the formation of atomic-scale structures on silicon surfaces[3], but the fabrication of working devices—such as transistors with extremely short gate lengths[4], spin-based quantum computers[5–8] and solitary dopant optoelectronic devices[9]—requires the ability to position individual atoms in a silicon crystal with atomic precision. Here, we use a combination of scanning tunnelling microscopy and hydrogen-resist lithography to demonstrate a single-atom transistor in which an individual phosphorus dopant atom has been deterministically placed within an epitaxial silicon device architecture with a spatial accuracy of one lattice site. The transistor operates at liquid helium temperatures, and millikelvin electron transport measurements confirm the presence of discrete quantum levels in the energy spectrum of the phosphorus atom. We find a charging energy that is close to the bulk value, previously only observed by optical spectroscopy[10].

Silicon technology is now approaching a scale at which both the number and location of individual dopant atoms within a device will determine its characteristics[11], and the variability in device performance caused by the statistical nature of dopant placement[12] is expected to impose a limit on scaling before the physical limits associated with lithography and quantum effects[13] are reached. Controlling the precise position of dopants within a device and understanding how this affects device behaviour have therefore become essential[14–17]. Devices based on the deterministic placement of single dopants in silicon are also leading candidates for solid-state quantum computing architectures, because the dopants can have extremely long spin-coherence[18] and spin-relaxation times[19], and because this approach would be compatible with existing complementary metal-oxide-semiconductor (CMOS) technology.

One of the earliest proposals for a solid-state quantum computer involved arrays of single ^{31}P atoms in a silicon crystal, with the two nuclear spin states of the ^{31}P atom providing the basis for a quantum bit (qubit)[5]. Subsequently, qubits based on the electron spin states[6,7] or charge degrees of freedom[20] of dopants in silicon were proposed. This has led to increased interest in measuring the electronic spectrum of individual dopants in field-effect transistor architectures, where the dopants are introduced by low-energy implantation[16] or in-diffusion from highly doped contact regions[14,15,17]. However, these approaches are limited to a precision of ~10 nm in the position of the dopants, and the practical implementation of a quantum computing device based on this approach requires the ability to place individual phosphorus atoms into silicon with atomic precision[21] and to register electrostatic gates and readout devices to each individual dopant.

Figure 1 shows the approach we used to deterministically place a single phosphorus atom between highly phosphorus-doped source and drain leads in a planar, gated, single-crystal silicon transport device. This involved the use of hydrogen-resist lithography[22–24] to

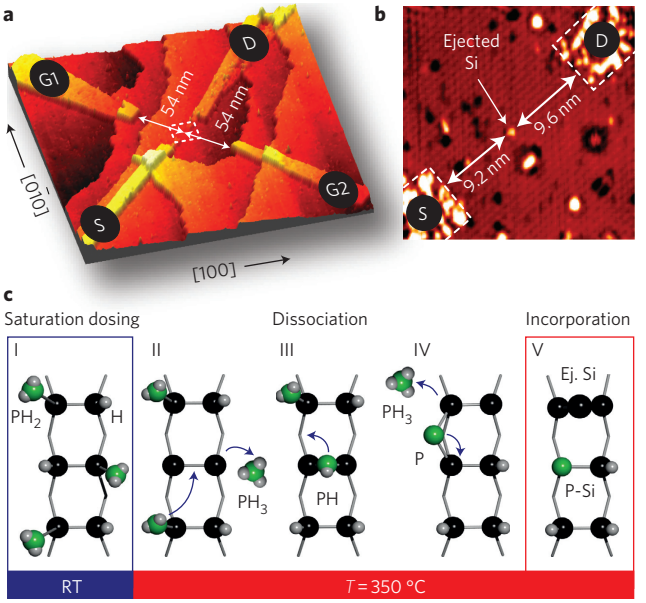

Figure 1 | Single-atom transistor based on deterministic positioning of a phosphorus atom in epitaxial silicon. a, Perspective STM image of the device, in which the hydrogen-desorbed regions defining source (S) and drain (D) leads and two gates (G1, G2) appear raised due to the increased tunnelling current through the silicon dangling bond states that were created. Upon subsequent dosing with phosphine, these regions form highly phosphorus-doped co-planar transport electrodes of monatomic height, which are registered to a single phosphorus atom in the centre of the device. Several atomic steps running across the Si(100) surface are also visible. **b**, Close-up of the inner device area (dashed box in **a**), where the central bright protrusion is the silicon atom, which is ejected when a single phosphorus atom incorporates into the surface. **c**, Schematic of the chemical reaction to deterministically incorporate a single phosphorus atom into the surface. Saturation dosing of a three-dimer patch (I) at room temperature (RT) followed by annealing to 350 °C allows successive dissociation of PH_3 (II–IV) and subsequent incorporation of a single phosphorus atom in the surface layer, ejecting a silicon adatom in the process (V).

[1]Centre for Quantum Computation and Communication Technology, School of Physics, University of New South Wales, Sydney, NSW 2052, Australia, [2]Supercomputing Center, Korea Institute of Science and Technology Information, Daejeon 305-806, South Korea, [3]Network for Computational Nanotechnology, Birck Nanotechnology Center, Purdue University, West Lafayette, Indiana 47907, USA, [4]Centre for Quantum Computation and Communication Technology, School of Physics, University of Sydney, Sydney NSW 2006, Australia, [5]Centre for Quantum Computation and Communication Technology, School of Physics, University of Melbourne, Parkville, VIC 3010, Australia. *e-mail: michelle.simmons@unsw.edu.au

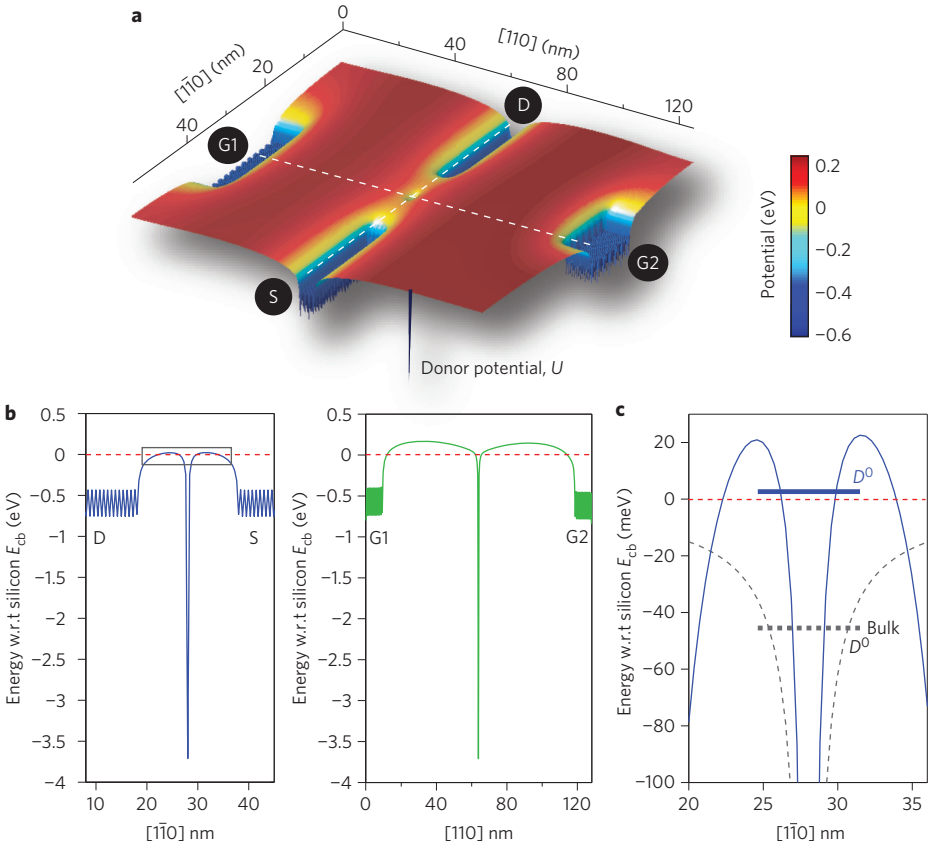

Figure 2 | Calculation of the donor potential within the device architecture. a, False-colour plot showing how the calculated potential (at equilibrium) varies with position in the region between the highly doped electrodes. The superimposed donor potential *U* represents the single phosphorus atom in the centre of the device. **b**, Line profiles showing how the potential varies with position between the source and drain electrodes (left) and the two gate electrodes (right) (the position of the profiles are indicated by dashed white lines in **a**). The potential is plotted with respect to the conduction band-edge of bulk silicon, E_{cb}, indicated by the red dashed line. Apparent oscillations at the edges of the plots correspond to the phosphorus donor potentials within the highly doped electrodes, as represented by the self-consistent atomistic model. **c**, Close-up of the area indicated by the rectangle in the left panel of **b** comparing the potential profile between the source and drain electrodes in our device (blue line) to an isolated bulk phosphorus donor (dashed grey line), where the D^0 state resides 45.6 meV below E_{cb}. In contrast, the D^0 state in the single-atom transistor resides closer to the top of the potential barrier.

control the dissociation of the dopant precursor, phosphine (PH_3), before incorporation of the phosphorus atom at the required position in the silicon substrate. We found that three adjacent desorbed dimers (pairs of silicon surface atoms) along one dimer row result in the reliable incorporation of a single dopant, as illustrated in Fig. 1c. The incorporation pathway comprises a succession of well-understood dissociative processes[25] governed by the availability of bare silicon sites within the three-dimer patch. High dose rates at room temperature ensure that three PH_3 molecules dissociate within the three-dimer site into $PH_2 + H$, inhibiting any further reactions. Subsequent heating of the surface to 350 °C allows one PH_2 fragment to recombine with a hydrogen atom and desorb. The resulting availability of one free silicon site enables the immediate dissociation of another PH_2 to $PH + H$. Further reactions are inhibited until the final PH_2 recombines with H, creating another free site for the remaining PH to dissociate to P. Still at 350 °C, the phosphorus atom subsequently incorporates into the top layer of the silicon surface, resulting in the ejection of a silicon adatom (Fig. 1c, part V). The incorporated phosphorus atom therefore substitutes for one of the six silicon atoms within the designated three-dimer patch, which translates to a lateral spatial positioning accuracy of ± 1 lattice site (± 3.8 Å).

The properties of isolated dopants in bulk silicon are well understood[10], but transport devices such as transistors contain electrodes that have profound effects on the energetics of single dopant atoms[14]. To tune the electrostatic potential at the position of the dopant, two in-plane gates G1 and G2 were patterned on either side of the transport channel defined by the S and D leads, at a distance of 54 nm from the central donor (Fig. 1a). All four planar electrodes were highly phosphorus-doped and therefore conducted at cryogenic temperatures, while the surrounding low-doped substrate became insulating as a result of carrier freeze-out[24]. Both the tunnel coupling of the donor to the leads as well as the capacitive coupling to the gates are determined by the device architecture, which can be controlled with atomic precision by scanning tunnelling microscope (STM)–lithography.

To understand quantitatively how the nearby transport electrodes affect the electronic properties of the donor, we have calculated the electrostatic potential landscape of the innermost part of the device, treating the heavily doped gate regions in a self-consistent atomistic approach (see Methods) using a Thomas–Fermi approximation. This is illustrated for equilibrium conditions (that is, no biases applied to the gates) in Fig. 2a, in which we find that the presence of highly doped electrodes strongly alters the usual Coulombic potential of the donor. This can be seen in the two perpendicular line cuts along the S–D and G1–G2 axes, respectively (Fig. 2b), which illustrate the anisotropy of the donor potential in our device, with electrodes closer to the donor resulting in shallower barriers. Here, the potential within the leads (at the edges of these traces) remains below the conduction band-edge of bulk silicon due to the high doping density in the electrodes. The float-up of the central electrostatic potential arises from the very large gradient

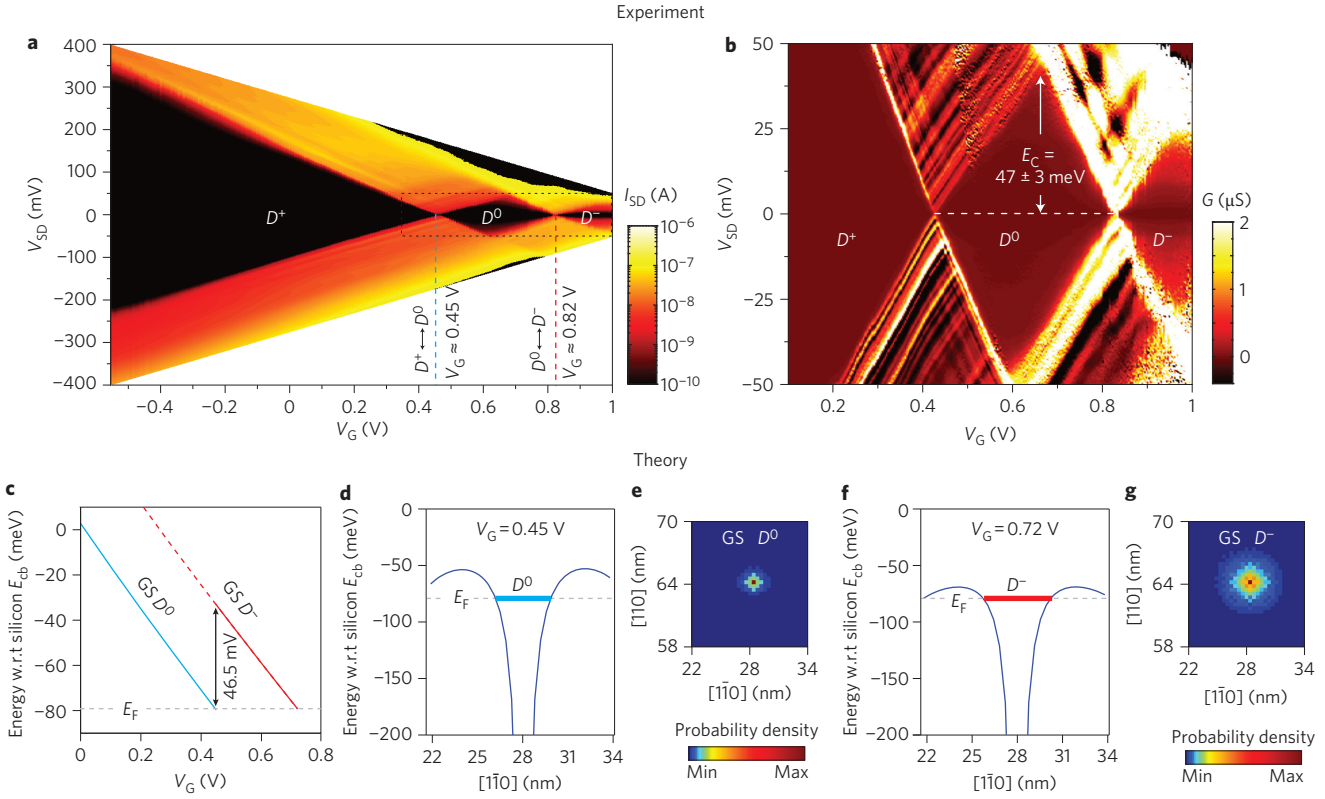

Figure 3 | Electronic spectrum of a single-atom transistor. a, Stability diagram showing the drain current I_{SD} (on a logarithmic scale) as a function of source–drain bias V_{SD} and gate voltage V_G (applied to both gates in parallel). The $D^+ \rightarrow D^0$ and $D^0 \rightarrow D^-$ transitions occur reproducibly at $V_G \approx 0.45$ V and 0.82 V, respectively. **b**, Differential conductance dI_{SD}/dV_{SD} (on a linear scale) as a function of V_{SD} and V_G in the region of the D^0 diamond shown in **a**. From this we determine the charging energy E_c to be $\sim 47 \pm 3$ meV. **c**, Calculated energies of the D^0 and D^- ground states (GS) as a function of V_G. The difference in the energy of these two ground states gives a charging energy of $E_c \approx 46.5$ meV, which is in excellent agreement with experiment. Charge transitions occur when a ground state crosses the Fermi level (E_F) in the leads. **d**–**g**, Potential profiles between source and drain electrodes calculated for $V_G = 0.45$ V (**d**) and 0.72 V (**f**). The effective barrier height is lower for the higher value of V_G. The calculated orbital probability density of the ground state for the D^0 potential (**e**) is more localized around the donor than for the D^- potential (**g**), which is screened by the bound electron.

in the free charge and has previously been observed in resonant tunnelling diodes[26].

Having established the electrostatic potential of the device, we then calculated the donor electronic states using a tight-binding approach[14]. The position of the resulting one-electron ground state D^0 for the solitary phosphorus dopant is depicted in Fig. 2c (blue line). As expected, due to the electrostatic environment, the energy levels of our device are raised significantly from the bulk case (dashed grey line), where the unperturbed Coulombic donor potential asymptotically approaches the silicon conduction band minimum E_{cb} (red dashed line) and D^0 has a binding energy[10] of $E_B \approx -45.6$ meV. In contrast, D^0 in the effective donor potential of our transport device resides much closer to the top of the barrier (solid line) along the S–D transport direction. However, it is important to note that—in contrast to the bulk case—the binding energy in our device is not simply given by the separation between the donor levels and the top of the barrier along S–D. This is because the donor resides in an anisotropic potential, as shown in Fig. 2b, with stronger confinement along the transverse (G1–G2) direction. Because the binding energies are not accessible in our device (as a result of the limited gate range), we therefore calculated the charging energy, that is, the energy difference between D^0 and the two-electron D^- state, which can be directly determined from the transport data.

Figure 3a presents the measured stability diagram of the single donor, in which we can easily identify three charge states of the donor: the ionized D^+ state, the neutral D^0 state and the negatively charged D^- state. The diamond below $V_G \approx 0.45$ V does not close, as expected[14] for the ionized D^+ state, because a donor cannot lose more than its one valence electron. The conductance remains high (on the order of microsiemens) down to the lower end of the gating range, making the possibility of additional charge transitions unlikely. Importantly, the $D^+ \leftrightarrow D^0$ charge transition occurs reproducibly at $V_G = 0.45 \pm 0.03$ V for multiple cool-downs of the device. This consistent behaviour is a testament to the high stability of the device and the inherent influence of the nearby electrodes on the position of the donor eigenstates relative to the Fermi level of the leads. The detuning of these states as a function of gate voltage (with both gates at the same potential) is calculated self-consistently for the potential landscape of our device (Fig. 3c), and we find that the D^0 level (blue line) shifts downwards linearly as a function of gate voltage. We note that the Fermi level (E_F) in the leads is pulled ~ 80 meV below the conduction band minimum of bulk silicon due to the extremely high doping density. The first charge transition within our model, when one electron occupies the donor, occurs when the D^0 level aligns with the Fermi level, at $V_G = 0.45$ V. The agreement with the experimental value is striking, in particular as no fitting parameters for our device were used in our calculations—only the actual device dimensions. At this gate bias ($V_G = 0.45$ V), the barrier height is significantly reduced along the transport direction (Fig. 3d) compared to the equilibrium case (Fig. 2c). This results from the non-proximal coupling of the gates; the applied gate voltage shifts the electrochemical potential of the donor states and also modulates the potential landscape between the donor and the leads.

At $V_G > 0.45$ V, the bound electron effectively screens the donor core potential. We can account for this theoretically by self-consistently filling the initial Coulomb potential with one electron. The resulting D^- state is thus much closer to the top of the barrier along the transport direction (Fig. 3f), and the corresponding orbital probability density (Fig. 3g) is considerably less localized than in the D^0 case (Fig. 3e). However, the remaining effective barrier (~12 meV) and strong confinement in the G1–G2 direction explains the larger extent of the D^- region in Fig. 3b, which exceeds the value expected for a bulk donor (~1.7 meV).

For the screened donor potential, we again calculated the shift of the D^- level as a function of gate voltage. We found that the D^- state comes into resonance with E_F at $V_G = 0.72$ V (Fig. 3c), close to the experimentally observed V_G value from Fig. 3a. The discrepancy with respect to the experimental value (~0.82 V) for this second charge transition is probably due to necessary simplifications in our modelling approach. In particular, by neglecting depletion effects arising from band bending[26] at the edges of the highly doped gate electrodes at positive gate voltages, our model overestimates the effective lever arm, which is a measure for the electrostatic coupling strength between the gates and the donor. Because the depletion effect increases with applied gate voltage, the deviation is expected to be more significant for the second charge transition, which occurs at a higher value of V_G.

Importantly, from the transport data of Fig. 3, we can determine the charging energy (E_c), and compare this with values extracted from absorption spectroscopy[10] for a bulk donor in silicon. From a close-up of the stability diagram in Fig. 3b we can extract a charging energy of 47 ± 3 meV, in which the error arises from the asymmetry of the diamond height for $V_{SD} > 0$ and $V_{SD} < 0$ resulting from the different capacitive coupling of the one- and two-electron donor states to the electrodes. Despite the presence of nearby electrodes, the experimental value for E_c in our device is remarkably similar to the value expected for isolated phosphorus donors based on the binding energies (45.6 meV for D^0 and ~1.7 meV for D^-, respectively)[10] in bulk silicon. This is in sharp contrast to previous experiments on single dopant in silicon transport devices, which have reported charging energies that significantly differ from the bulk case[14,17,27]. There, the difference was attributed either to screening effects resulting from strong capacitive coupling to a nearby gate[14] or strong electric fields[27], or to an enhanced donor ionization energy in the proximity of a dielectric interface[17]. Importantly, these effects are expected to be small for our phosphorus dopant, which is symmetrically positioned between the two gates and encapsulated deep within an epitaxial silicon environment. The bulk-like charging energy observed experimentally is fully supported by the modelling (Fig. 3c), in which E_c is given by the energy separation between the D^0 and D^- states. The calculated value of 46.5 meV is slightly larger than the ~44 meV expected from the binding energies determined for the bulk case[10], and probably results from the artificial confinement represented by the simulation domain boundaries in our model[27] (see Methods), which overestimates the energy for D^-. At the same time, the presence of electron–electron interactions, which are not fully captured by the mean-field self-consistent method[27] to calculate the effective D^- potential, may also contribute to the slight discrepancy between calculated and experimental values.

We have fabricated a single-atom transistor in which a single phosphorus atom is positioned between highly doped source and drain leads with a lateral spatial accuracy of ± 1 atomic lattice spacing. We demonstrate that we are able to register source, drain and gate contacts to the individual donor atom and observe well-controlled transitions for 0, 1 and 2 electron states, in agreement with atomistic modelling of the device. Our results show that encapsulating phosphorus dopant atoms deep within an epitaxial silicon environment allows them to retain both their discrete quantum states and their bulk-like charging energy, despite the presence of highly doped electrodes. These results demonstrate that single-atom devices can in principle be built and controlled with atomically thin wires, where the active component represents the ultimate physical limit of Moore's law. As such, these results are highly relevant to the development of atomic-scale silicon transistors, and our approach could also be applied to the fabrication of single-dopant optoelectronic devices and spin-based quantum computation.

Methods

The STM was used in lithography mode to selectively desorb the hydrogen resist on the Si(100)-2 × 1 surface of a p-type (boron) low-doped substrate. The planar device structure was defined in two steps. First, the innermost parts of the leads and the central three-dimer patch were desorbed, PH_3-dosed at 14 langmuir, and annealed for 5 s at 350 °C. The outer structures (gates, lead extensions and micrometre-sized contact patches) were aligned and desorbed, PH_3-dosed at ~1.4 langmuir, followed by a 60 s incorporation anneal at 350 °C. The entire structure was then overgrown with ~180 nm silicon from a sublimation source, with the sample held at 250 °C. Electrical measurements were carried out in a $^3He/^4He$ dilution refrigerator at base temperature (~20 mK) with a d.c. voltage V_{SD} applied to the S electrode while keeping D grounded.

An atomistic tight-binding approach implemented in NEMO-3D (Nanoelectronic Modeling tool)[28] was used to generate the electrostatic potential[26] and Fermi energy of the highly doped leads[29,30] in a self-consistent manner for a range of gate biases. A Coulomb potential (U) was then superimposed on the potential landscape to represent the quantum confinement of the solitary phosphorus dopant in the transport channel. Different calculated potentials were used at the appropriate gate biases to represent the one-electron ground state D^0 and the two-electron D^- state. The fully characterized electrostatic environment coupled with a tight-binding Schrödinger solver was used to calculate the eigenstates of the deterministically placed dopant. The simulation domain used to calculate the donor potential was limited along S–D (but included the barrier maxima regions) to prevent the formation of artificial potential wells and consequently charge accumulation at the edges.

Received 16 December 2011; accepted 26 January 2012; published online 19 February 2012

References

1. Binnig, G., Rohrer, H., Gerber, C. & Weibel, E. Tunneling through a controllable vacuum gap. *Appl. Phys. Lett.* **40,** 178–180 (1982).
2. Eigler, D. M. & Schweizer, E. K. Positioning single atoms with a scanning tunnelling microscope. *Nature* **344,** 524–526 (1990).
3. Lopinski, G. P., Wayner, D. D. M. & Wolkow, R. A. Self-directed growth of molecular nanostructures on silicon. *Nature* **406,** 48–51 (2000).
4. Frank, D. J. *et al.* Device scaling limits of Si MOSFETs and their application dependencies. *Proc. IEEE* **89,** 259–288 (2001).
5. Kane, B. E. A silicon-based nuclear spin quantum computer. *Nature* **393,** 133–137 (1998).
6. Vrijen, R. *et al.* Electron-spin-resonance transistors for quantum computing in silicon–germanium heterostructures. *Phys. Rev. A* **62,** 012306 (2000).
7. Hollenberg, L. C. L., Greentree, A. D., Fowler, A. G. & Wellard, C. J. Two dimensional architectures for donor based quantum computing. *Phys. Rev. B* **74,** 045311 (2006).
8. Morton, J. J. L., McCamey, D. R., Eriksson, M. A. & Lyon, S. A. Embracing the quantum limit in silicon computing. *Nature* **479,** 345–353 (2011).
9. Koenraad, P. M. & Flatté, M. E. Single dopants in semiconductors. *Nature Mater.* **10,** 91–100 (2011).
10. Ramdas, A. K. & Rodriguez, S. Spectroscopy of the solid-state analogs of the hydrogen atom: donors and acceptors in semiconductors. *Rep. Prog. Phys.* **44,** 1297–1387 (1981).
11. Roy, S. & Asenov, A. Where do the dopants go? *Science* **309,** 388–390 (2005).
12. Shinada, T., Okamoto, S., Kobayashi, T. & Ohdomari, I. Enhancing semiconductor device performance using ordered dopant arrays. *Nature* **437,** 1128–1131 (2005).
13. Zhirnov, V. V., Cavin, R. K., Hutchby, J. A. & Bourianoff, G. I. Limits to binary logic switch scaling—a Gedanken model. *Proc. IEEE* **91,** 1934–1939 (2003).
14. Lansbergen, G. P. *et al.* Gate-induced quantum-confinement transition of a single dopant atom in a silicon FinFET. *Nature Phys.* **4,** 656–661 (2008).
15. Calvet, L. E., Snyder, J. P. & Wernsdorfer, W. Excited-state spectroscopy of single Pt atoms in Si. *Phys. Rev. B* **78,** 195309 (2008).
16. Tan, K. Y. *et al.* Transport spectroscopy of single phosphorus donors in a silicon nanoscale transistor. *Nano Lett.* **10,** 11–15 (2010).
17. Pierre, M. *et al.* Single-donor ionization energies in a nanoscale CMOS channel. *Nature Nanotech.* **5,** 133–137 (2010).
18. Tyryshkin, A. M. *et al.* Electron spin coherence exceeding seconds in high-purity silicon. *Nature Mater.* **11,** 143–147 (2012).

19. Morello, A. *et al.* Single-shot readout of an electron spin in silicon. *Nature* **467,** 687–691 (2010).
20. Hollenberg, L. C. L. *et al.* Charge-based quantum computing using single donors in semiconductors. *Phys. Rev. B* **69,** 113301 (2004).
21. Koiller, B., Hu, X. D. & Das Sarma, S. Exchange in silicon-based quantum computer architecture. *Phys. Rev. Lett.* **88,** 027903 (2002).
22. Lyding, J. W., Shen, T. C., Hubacek, J. S., Tucker, J. R. & Abeln, G. C. Nanoscale patterning and oxidation of H-passivated Si(100)-2×1 surfaces with an ultrahigh-vacuum scanning tunneling microscope. *Appl. Phys. Lett.* **64,** 2010–2012 (1994).
23. Schofield, S. R. *et al.* Atomically precise placement of single dopants in Si. *Phys. Rev. Lett.* **91,** 136104 (2003).
24. Fuhrer, A., Füchsle, M., Reusch, T. C. G., Weber, B. & Simmons, M. Y. Atomic-scale, all epitaxial in-plane gated donor quantum dot in silicon. *Nano Lett.* **9,** 707–710 (2009).
25. Wilson, H. F. *et al.* Thermal dissociation and desorption of PH_3 on Si(001): a reinterpretation of spectroscopic data. *Phys. Rev. B* **74,** 195310 (2006).
26. Klimeck, G., Lake, R., Bowen, R. C., Frensley, W. R. & Moise, T. S. Quantum device simulation with a generalized tunneling formula. *Appl. Phys. Lett.* **67,** 2539–2541 (1995).
27. Rahman, R. *et al.* Electric field reduced charging energies and two-electron bound excited states of single donors in silicon. *Phys. Rev. B* **84,** 115428 (2011).
28. Klimeck, G., Oyafuso, F., Boykin, T. B., Bowen, R. C. & von Allmen, P. Development of a nanoelectronic 3D (NEMO 3D) simulator for multimillion atom simulations and its application to alloyed quantum dots. *Comput. Model. Eng. Sci.* **3,** 601–642 (2002).
29. Lee, S. *et al.* Electronic structure of realistically extended, atomistically resolved disordered Si:P δ-doped layers. *Phys. Rev. B* **84,** 205309 (2011).
30. Weber, B. *et al.* Ohm's law survives to the atomic scale. *Science* **335,** 64–67 (2012).

Acknowledgements

The authors acknowledge discussions with S. Rogge, J. Verduijn and R. Rahman. This research was conducted by the Australian Research Council Centre of Excellence for Quantum Computation and Communication Technology (project no. CE110001027). The research was also supported by the US National Security Agency and the US Army Research Office (contract no. W911NF-08-1-0527). M.Y.S. acknowledges a Federation Fellowship. L.H. acknowledges an Australian Professorial Fellowship.

Author contributions

M.F. and J.M. carried out the fabrication and measurements. M.F., J.M., S.M., O.W., M.S., G.K. and L.H. analysed the data. H.R. and S.L. carried out the calculations. M.S. planned the project. G.K. and L.H. planned the modelling approach. M.F., J.M., S.M., H.R., G.K., L.H. and M.S. prepared the manuscript.

Additional information

The authors declare no competing financial interests. Reprints and permission information is available online at http://www.nature.com/reprints. Correspondence and requests for materials should be addressed to M.Y.S.